

## Article

# Assessment of Cytochrome c and Chlorophyll a as Natural Redox Mediators for Enzymatic Biofuel Cells Powered by Glucose

Urte Samukaite Bubniene <sup>1,2,3,\*</sup>, Sarunas Zukauskas <sup>2</sup>, Vilma Ratautaite <sup>1,2</sup>, Monika Vilkiene <sup>4</sup>, Ieva Mockeviciene <sup>4</sup>, Viktorija Liustrovaite <sup>2</sup>, Maryia Drobysh <sup>1,2</sup>, Aurimas Lisauskas <sup>5</sup>, Simonas Ramanavicius <sup>2,6</sup> and Arunas Ramanavicius <sup>1,2,\*</sup>

- <sup>1</sup> Department of Nanotechnology, State Research Institute Center for Physical Sciences and Technology (FTMC), Sauletekio av. 3, LT-10257 Vilnius, Lithuania
  - <sup>2</sup> Department of Physical Chemistry, Institute of Chemistry, Faculty of Chemistry and Geosciences, Vilnius University, Naugarduko Str. 24, LT-03225 Vilnius, Lithuania
  - <sup>3</sup> Department of Mechatronics, Robotics and Digital Manufacturing, Faculty of Mechanics, Vilnius Gediminas Technical University, J. Basanaviciaus Str. 28, LT-03224 Vilnius, Lithuania
  - <sup>4</sup> Institute of Agriculture, Lithuanian Research Center for Agriculture and Forestry (LAMMC), Vezaiciai Branch, Gargzdu Str. 29, Klaipeda district, LT-96216 Vezaiciai, Lithuania
  - <sup>5</sup> Laboratory of Combustion Processes, Lithuanian Energy Institute, Breslaujos Str. 3, LT-44403 Kaunas, Lithuania
  - <sup>6</sup> Department of Electrochemical Material Science, State Research Institute Center for Physical Sciences and Technology (FTMC), Sauletekio av. 3, LT-10257 Vilnius, Lithuania
- \* Correspondence: urte.bubniene@ftmc.lt or urte.samukaite-bubniene@chf.vu.lt (U.S.B.); arunas.ramanavicius@chf.vu.lt or arunas.ramanavicius@ftmc.lt (A.R.)



**Citation:** Samukaite Bubniene, U.; Zukauskas, S.; Ratautaite, V.; Vilkiene, M.; Mockeviciene, I.; Liustrovaite, V.; Drobysh, M.; Lisauskas, A.; Ramanavicius, S.; Ramanavicius, A. Assessment of Cytochrome c and Chlorophyll a as Natural Redox Mediators for Enzymatic Biofuel Cells Powered by Glucose. *Energies* **2022**, *15*, 6838. <https://doi.org/10.3390/en15186838>

Academic Editor: Attilio Conventi

Received: 11 August 2022

Accepted: 11 September 2022

Published: 19 September 2022

**Publisher's Note:** MDPI stays neutral with regard to jurisdictional claims in published maps and institutional affiliations.



**Copyright:** © 2022 by the authors. Licensee MDPI, Basel, Switzerland. This article is an open access article distributed under the terms and conditions of the Creative Commons Attribution (CC BY) license (<https://creativecommons.org/licenses/by/4.0/>).

**Abstract:** The development of new high-power biofuel cells has been limited in the past by slow or indirect charge transfer. In this study, enzymatic biofuel cell (EBFC) systems were explored with different materials used to evaluate their applicability as redox mediators. Redox mediators of different natures have been selected for this research. Cytochrome c, Chlorophyll a, and supernatant of ultrasonically disrupted algae *Chlorella vulgaris* cells were examined as potential redox mediators. The effect of heparin on the EBFC was also evaluated under the same analytical conditions. The measurements of open circuit potential (OCP) and the evaluation of the current response in two modes of measurement were performed (i) during potential cycling in cyclic voltammetry measurements or (ii) at the constant potential value in chronoamperometry, and were applied for the evaluation of EBFC. Cytochrome c, Chlorophyll a, and the supernatant of ultrasonically disrupted algae *Chlorella vulgaris* cells-based redox mediators were efficient in the glucose oxidase (GOx) based EBFC. Electron transfer from GOx to the electrode was facilitated through the redox mediators adsorbed on the electrode. Electrodes modified with Chlorophyll a- and Cytochrome c-based redox mediators were suitable for the development of glucose biosensors. This was demonstrated by increasing the glucose concentration within 0 mM–100 mM in the system, the current density increased, and the system reached equilibrium rather faster regarding the electrochemical reaction. The power density is an important feature in revealing the action of biofuel cells. The highest power values were generated by the systems based on the application of redox-mediated Chlorophyll a and the supernatant of ultrasonically disrupted *Chlorella vulgaris* cells. The surface power density was about 2.5–4.0  $\mu\text{W}/\text{cm}^2$ . Control of a study was performed with a polished graphite electrode and the maximum surface power density was 0.02471  $\mu\text{W}/\text{cm}^2$ .

**Keywords:** microbial-based biofuel cell; redox mediators; cytochrome c; the supernatant of ultrasonically disrupted *Chlorella vulgaris* cells; Chlorophyll a; heparin; glucose

## 1. Introduction

Electricity is not only essential for the well-being of industry, commerce, and society but personal convenience and mobility. However, the scale of electricity consumption and generation is a cause for concern [1]. With the increasing growth in the household, industry, transportation, and implantable device markets, the demand for backup power generation has increased tremendously. Human activity has the greatest impact on electricity demand, which was seen during the coronavirus SARS-CoV-2-induced disease 2019 (COVID-19) lockdowns [2–4]. The dwindling reserves of non-renewable fossil fuels are encouraging the search for commercially viable alternatives to electricity sources, which would also assist in solving environmental pollution problems. Biological fuel cells are an ecological alternative for the generation of electrical current [5]. They are ecological, renewable, and do not pollute nature. Because of their biocompatibility, biofuel cells are a desirable power source for microscale and implanted medical devices.

There are two types of biofuel cells—microorganism-based biofuel cells [6] and enzyme-based biofuel cells [7]. An excellent feature of enzymes, as catalysts, is that they are highly selective, because they only catalyse specific reactions, therefore, most of them are harmless, active at room and/or human body temperature, and at near to neutral pH values, hence they can be compatible with living organisms. In addition, most biofuel cells are powered by renewable fuels such as ethanol, glucose, sucrose, glycerol, acetate, phenol, lactate, ribitol, and organics present in wastewater, etc. [8,9].

Among the types of enzymatic biofuel cells, glucose biofuel cells are the most widely studied by scientists and have the greatest potential for practical application, as living organisms have enough glucose and oxygen to function in such systems, and these substances are constantly renewed [10]. One of the advantages is that biofuel cells can produce more energy than conventional batteries because the fuel in the system can be constantly renewed almost without any limitations, which makes such systems very attractive. However, relatively low power output is still being exhibited. To overcome this problem, redox mediators are introduced into the system.

High fuel cell standards require that a biofuel cell must be simple, efficient, long-lasting, stable, easily compatible, and most importantly, commercially viable. Different efficiencies can be obtained by changing the types of electrodes [11], their modification methods [12], the composition of the buffer solutions [13,14], enzymes themselves [15], and mediators used [16]. A considerable amount of research to make this fuel-producing equipment economically viable is spent and systems are being improved in various ways.

The enzymatic fuel cell can be mediated and unmediated (Figure 1). Most enzyme-based cells are electrochemically active, although charge exchange between an enzyme and an electrode can be facilitated more effectively via the mediators.

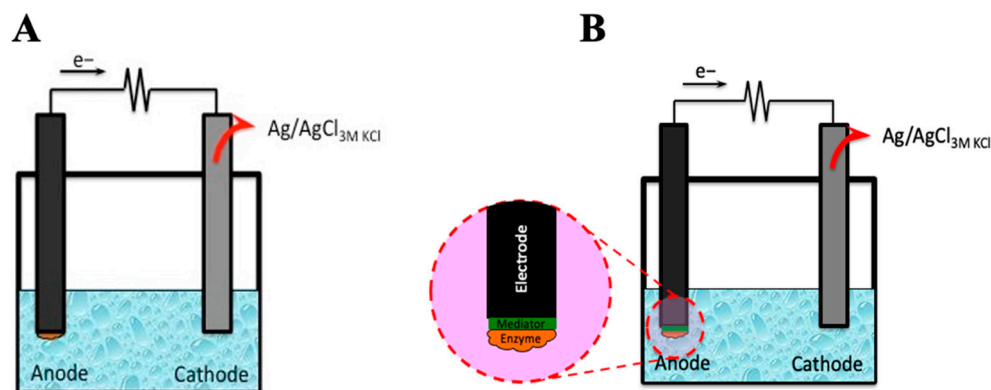


**Figure 1.** Principal scheme of (A) enzyme-based mediator-free biofuel cell and (B) mediated enzyme-based biofuel cell.

The efficiency of charge transfer between the reactive site of the enzyme and the electrode surface is a key feature of enzymatic biofuel cells. The velocity of this process is crucial for creating effective enzymatic biofuel cells, and the electrochemical reaction rate determines how well they will operate. Enzymatic biofuel cells are of two primary categories based on the methodology that enables charge transfer between particular electrodes and enzymes. The categories are based on: (i) direct electron transfer (DET) [17], where the enzyme can transfer charge towards the electrode directly, and (ii) mediated electron transfer (MET), which utilizes immobilized redox mediators or redox mediators dissolved in solution to transport electrons toward the electrode surface [18]. However, a rather slow charge transfer between the enzyme and the electrode is the main issue, which is assessed by researchers developing enzymatic fuel cells. Consequently, improving charge transfer between the different elements of these devices is one of the most crucial tasks for the development of biofuel cells and some other devices that are based on bioelectronics. To mediate charge shuttling between the enzyme and electrode surface, various redox compounds include hierarchical nanoporous carbon [17], gold nanoparticles [19,20], gold nanoclusters [9], and platinum-based nanoparticles [21]. In addition, redox compounds of low molecular weight, such as cytochromes, are exploited as redox mediators [22]. The use of a mediator in fuel cell systems provides for higher power generation and just rather low interference effects at a lower cell potential. Moreover, a redox mediator should have the following properties: rapid electrochemical kinetics and a rather stable oxidation state [16].

In previous studies, the following mediators were described [7]: phenanthrenequinone [23], ubiquinone/ubiquinol [24] ferrocene methanol, methylene blue or 2,2'-azinobis(3-ethylbenzothiazoline-6-sulfonic acid) [25], 9,10-phenanthroline-5,6-dione [7], and methyl-1,4-naphthoquinone [26], all used as anodic redox mediators. Several aspects should be carefully considered while selecting appropriate redox mediators for microbial biofuel cells. One of them is the solubility of a mediator in the media. Mediators are categorized according to their solubility in water-based media or organic solvent-based media. The most often-used example of the hydrophilic mediator is potassium ferricyanide/ferrocyanide. In the case of microbial biofuel cells, the examples of lipophilic redox mediators are 1,10-phenanthroline-5,6-dione or 9,10-phenanthrenequinone. Lipophilic redox mediators (e.g., 1,10-phenanthroline-5,6-dione) are able to penetrate cell membranes and shuttle an electric charge through cellular membranes. Our research team [6] has described an application of a system based on the action of two-redox mediators. Additionally, microbial cells in this study were encapsulated within conducting polymer polypyrrole. Two redox mediator systems of  $\text{Fe}(\text{CN})_6^{3-}/\text{Fe}(\text{CN})_6^{4-}$  (ferricyanide/ferrocyanide) and oxidized/reduced forms of 9,10-phenanthrenequinone or 1,10-phenanthroline-5,6-dione were used to ensure an efficient charge transfer. Such a mediator system allowed the generation of a current nearly three times higher in contrast to that observed for cells, which have not been modified.

Some polymers may be used to increase charge transfer. One of them is the polypyrrole [6,27]. Electropolymerized 'neutral red' was used as a redox mediator for the yeast-based fuel cell [28]. In that study, poly(neutral red) was electropolymerized by cyclic voltammetry on a carbon felt surface and during this electro-polymerization procedure, *Saccharomyces cerevisiae* cells were entrapped within the film. Other polymers used as bioanodes in biofuel cells are poly(methylene green) [29] or enzymatic fuel cells made of poly(methylene blue) and carbon nanotubes composite and powered by glucose/oxygen [30]. As it was stated by Conzuelo et al. [31], the electron mediator is covalently attached to a polymer chain.

Cytochromes are heme-based proteins, designed for charge transfer. The transfer of electrons is facilitated by an oscillation of the heme iron between the ferrous and the ferric forms [32] (Equation (1)):



A hemoprotein is a protein containing a heme prosthetic group. These proteins belong to a very large group of metalloproteins. The functionality provided by the hemoproteins in-

cludes oxygen-carrying, oxygen reduction, electron transfer, and some other effects [22,32]. The iron cation, typically  $\text{Fe}^{2+}$  or  $\text{Fe}^{3+}$ , is bound at the center of the conjugate base of the porphyrin and other ligands are coupled to the ‘axial sites’ of the iron to form the active site of heme. Oxygen transport is one of the many biological roles carried out by hemoproteins, namely, hemoglobin, myoglobin, leghemoglobin, cytoglobin, and neuroglobin. Some hemoproteins have enzymatic activity, e.g., cytochrome c oxidase, cytochrome P450s, peroxidases, ligninases, and catalase. They usually activate  $\text{O}_2$  for oxidation or hydroxylation. Hemoproteins also facilitate electron transfer, since many of them are components of the electron transfer chain. Cytochromes a, b, and c possess electron transport functions [33], which can be well exploited in biofuel cells [22]. Due to their oxidative reducing properties, hemoproteins are good electron carriers and, therefore, are mutual intermediaries between the electrode and the enzyme. Heme-based proteins are also less sensitive to halogen ions (e.g., fluoride and/or chloride) compared to some enzymes such as laccase, and chloride ions are known to be found in numerous biofuel cell systems [22].

Heparin, a highly sulfated glycosaminoglycan, has been utilized as a clinical anticoagulant for almost 100 years [34]. The glycosaminoglycan family of compounds, which also comprises a number of closely related members, including heparin sulfate, includes the carbohydrate heparin. The pharmaceutical industry typically processes heparin from swine or bovine intestinal tissues, and its molecules are in the range of 2000–40,000 Daltons [35]. Initially, heparin was discovered to be involved in numerous cellular processes, but it has only lately become clear how significant this compound is for a variety of practical applications. The primary usage of heparin is related to its antithrombotic properties. It is specifically used to treat and prevent arterial thromboembolism, deep vein thrombosis, myocardial infarction, pulmonary emboli, and unstable angina. Heparin couples to the lysyl residues on antithrombin and increases the rate of the complex formation [36]. Since the beginning of the pandemic, heparin was widely used in the treatment of COVID-19 patients, because, most likely, heparin has some antiviral properties and lowers hypoxia and cytokine storm severity [37]. However, this medication can cause some side effects such as disorder, thrombocytopenia, and allergic reactions [38], therefore, it must be well assessed when developing such compatible drugs.

Chlorophylls are green pigments, which are widely distributed across the plant kingdom and are crucial to the photosynthetic process. Chlorophylls are found in diverse plants, algae, and cyanobacteria [39]. Chlorophyll is formed of carbon and nitrogen atoms, and a magnesium ion in the middle. Nearly all green components of plants, such as leaves and stems, contain chlorophyll located in chloroplasts. Chloroplasts often are called the ‘food factories’ of the plant cell, because they generate chemical energy in the form of glucose, which is required for all plant cells. Chlorophylls were originally divided into four classes: chlorophylls a, b, c, and d [40]. Later, a new form of chlorophyll—chlorophyll f—was identified in stromatolite, which is a hard rock structure created by cyanobacteria, and is found in western Australia [41].

Chlorophyll-based structures play a crucial role in photosynthesis. These pigments have a unique ability to capture light energy and to use it in the photolysis of water molecules to replenish the reductive capacity of cells, and this energy is necessary for the assimilation of carbon in the subsequent stages of photosynthesis. This pigment is used for a variety of anthropogenic purposes, e.g., chlorophyll can be used as a redox mediator [42]. Chlorophyll has many other activities that increase the potential required for the application in a variety of technological purposes. The fluorescence activity of chlorophyll makes it a very attractive material for the development of optical biosensors. Additionally, chlorophylls exhibit a mild lasing activity, which is valuable for the design of organics-based laser [43].

The supernatant of ultrasonically disrupted *Chlorella vulgaris* cells is one of the most significant green eukaryotic microalgae. These microalgae store significant quantities of lipids, particularly large sets of fatty acids, which is the best choice for the production of biofuels. The rate of biofuel production is growing rapidly, therefore, algae may be able

to produce a significant amount of biofuels [44]. In light of this, *Chlorella* sp. has been investigated intensively from the point of view of bioenergy. In addition, it was applied in the design of algae-based biofuel cells [45–47] and the supernatant of *Chlorella vulgaris* cells disrupted by ultrasound was used in biofuel cell cathode, where bacteria oxidized organic matter and generated redox potential,  $H^+$ , and  $CO_2$ . The supernatant of sonicated *Chlorella vulgaris* cells was used in the cathode of a biofuel cell and  $CO_2$  and nitrogen were generated, and  $O_2$  was produced, which acted as an electron acceptor during the generation of electrical current. In addition, to resolve electron acceptor restriction-related issues, photosynthesizing algae applied in the cathode will enable the absorption of  $CO_2$ , nitrogen, and phosphate [48]. Algae-based systems are efficient in the production of biomass because they grow rapidly and have higher photosynthetic efficiency in comparison to plant systems, which take longer to start up, develop slowly, and therefore, have significantly lower efficiency [49].

Glucose, as a fuel, has a special place in the development of biofuel cells. Glucose ( $C_6H_{12}O_6$ ) is a monosaccharide that belongs to a subcategory of carbohydrates. The majority of plants and algae produce glucose during photosynthesis. Glucose is involved in the structure of the most prevalent carbohydrate in the world, cellulose, which forms plant cell walls [50]. Hence, the benefit of glucose is that it is produced in large quantities by plants or during some industrial processes. Therefore, glucose is ideal as an ecological fuel suitable for application in the biofuel cells [51]. The advantages of glucose-powered biofuel cells are their extended lifespans, and their capacity to generate power in a natural environment [52]. Nevertheless, one of the key barriers to the practical application of biofuel cells is the low power density, which is caused by complicated charge transfer from the microbe to the electrode [7].

In this research, we have evaluated the applicability of several potential redox mediators, namely cytochromes, chlorophylls, and the supernatant of ultrasonically disrupted algae *Chlorella vulgaris* cells. The applicability of these materials as redox mediators was evaluated by means of power density, cyclic voltammetry, and chronoamperometry. During the evaluation of the cyclic voltammetry results, the focus was on the value of the potential at which oxidation is observed. Meanwhile, during the evaluation of chronoamperometry results, the focus was on the changes of current with respect to glucose concentration in the solution. Furthermore, the impact of heparin on the EBFC characteristics was also evaluated.

## 2. Materials and Methods

### 2.1. Chemicals

Glucose oxidase (*Aspergillus niger*) was purchased from Fluka (Buchs, Switzerland). The solution of 0.1 M consisted of phosphate buffer and 0.1 M. NaCl, KCl,  $Na_2HPO_4$ ,  $KH_2PO_4$ , D-(+)-glucose, and glutaraldehyde (50% V) were purchased from Carl Roth (Karlsruhe, Germany). Cytochrome c (electrophoresed from lysed spirulina cells) (Norsk institute for vannforskning, Oslo, Norway). Chlorophyll a was isolated from spinach leaves according to the extraction procedure below. *Chlorella vulgaris* preparation was performed according to the protocol: firstly, *Chlorella vulgaris* algal cells were disrupted ultrasonically, then the ultrasonicated cells were centrifuged; the supernatant remaining after centrifugation was used in the experiments 125  $\mu\text{g}/\text{mL}$  heparin medicinal product (manufactured by Rotexmedica GmbH Arzneimittelwerk, Trittau, Germany); ethanol (Riedel-de Haën, Seelze, Germany); deionized water.

### 2.2. Extraction of Chlorophyll a

Twenty mL of the methanol-toluene solution (molar ratio 2:8) were added to 7.2 g of spinach and ground using porcelain mortar. The obtained mixture was filtered using a Buchner funnel. A silicagel extraction and toluene were used to fill the column up to a depth of 15 cm, and then the filtrate, containing Chlorophyll a, was added. Toluene was used to clean the column before the collection of the yellow fraction containing carotenoids. The green fraction containing Chlorophyll a was recovered within 50 mL of methanol-toluene

solution. A separator funnel was used to separate the toluene and methanol solutions. Moreover, the toluene solution, containing dissolved Chlorophyll a, was evaporated. The extracted Chlorophyll a was then dissolved in methanol.

### 2.3. Preparation of Electrodes for Biofuel Cells

Graphite rods (purchased from Sigma–Aldrich, Berlin, Germany) (99.99%, diameter of 3 mm, active surface area of 7.1 mm<sup>2</sup>) were utilized as working electrodes. The electrodes were prepared by polishing them with abrasives until an even reflective surface was obtained. The surface area of the electrode was maintained using silicone tubing. Three µL of the assessed material solution and 5 µL of glucose oxidase were physically deposited on the polished graphite electrode surface. The liquid was left to evaporate, 70% of the original volume after evaporation, until we could observe a dry outer edge beginning to form on the electrode's surface. After most of the liquid evaporated, the system was placed in a chamber saturated with glutaraldehyde vapor to chemically bond the structure on the electrode. Such systems were indicated as EBFC<sub>CC</sub>—the system with Cytochrome c, EBFC<sub>CA</sub>—the system with Chlorophyll a, EBFC<sub>ChV</sub>—the system with the supernatant of ultrasonically disrupted *Chlorella vulgaris* cells, and EBFC<sub>Hep</sub>—the system with heparin. The prepared working electrodes were tested electrochemically. Ag/AgCl<sub>(3M KCl)</sub> was utilized as a reference electrode and platinum wire (with a diameter of 0.5 mm) as a counter electrode. Both electrodes were purchased from PalmSens (Houten, Netherlands).

### 2.4. Electrochemical Measurements Based on Cyclic Voltammetry and Chronoamperometry

Potentiostat-galvanostat PGSTAT 30 with specialized software NOVA 2.1 (Utrecht, The Netherlands) was used to perform all electrochemical measurements.

The electromotive force of the biofuel cells was measured in a two-electrode configuration by measuring the potential difference between working and reference electrode in an open circuit configuration. The system was considered to have reached equilibrium once the change in observable voltage was under 2% over a 5 min time span.

The solution of 0.1 M phosphate buffer and 0.1 M KCl was utilized in all experiments. The freshly prepared stock solutions of glucose were left for one day to achieve equilibrium between  $\alpha$  and  $\beta$  forms. Any required concentration of glucose was obtained from stock solutions of 0.1 M and 1 M prepared from D-(+)-glucose.

The power characteristics of the systems were analyzed by closing the circuit with a simulated load and measuring the voltage drop-off. The carbon composite resistors between the ranges of 1 k $\Omega$  and 10 M $\Omega$  were used to simulate a load as it was reported in previous research [26].

Cyclic voltammetry (CV) and chronoamperometry (CA) measurements were performed in a three-electrode cell: the graphite electrodes modified with assessed mediators were used as the working electrodes, Ag/AgCl<sub>(3M KCl)</sub> as reference electrode, and Pt wire as a counter electrode. The cyclic voltammetry aimed to evaluate the oxidative potential and the current density at varying glucose concentrations. Two cycles at the scan rate of 50 mV/s in the potential window from  $-1.5$  V to 1.5 V were performed per experiment. In all cases, only the second cycle was used for the comparison and evaluation of the electrodes. The obtained oxidative peak position was then used as the potential value for chronoamperometric measurements. At the initial phase of the chronoamperometric measurements, 30 min were provided for the system to reach equilibrium, afterwards, glucose was added to the electrolyte solution and the current response was measured once the current stabilized additional portion of glucose was added to determine a calibration curve. Electrolyte solutions were intensively saturated by N<sub>2</sub> bubbling for 2 h to remove oxygen from the solution and to eliminate the influence of oxygen during measurements.

## 3. Results and Discussion

In this research, attempts have been made to improve the biofuel cell by modification of electrodes. The adaptation of the redox mediator was used to improve the electron

transfer efficiency in the system. Three different materials were used in order to check the applicability to use as redox mediators EBFC<sub>CC</sub>—the system with Cytochrome c substrate, EBFC<sub>CA</sub>—the system with Chlorophyll a substrate, and EBFC<sub>ChV</sub>—the system with the supernatant of ultrasonically disrupted *Chlorella vulgaris* cells. Under the same conditions, the system with heparin (EBFC<sub>Hep</sub>) was examined.

### 3.1. Determination of Power Density

The stability of current, the maximum value of the power output, and a large electromotive force are three key features of the biofuel cell [31]. In this study, an attempt was first made to determine a system that generates sufficient power for the biofuel cell. Hence the power and surface power density of the biofuel cell were calculated using Ohm's law and power calculation formula based on the surface area of the graphite electrode. The whole-cell OCP was calculated via the following Equation (2) [53]:

$$OCP = (E_k - E_{ref}) - (E_a - E_{ref}) = E_k - E_a \quad (2)$$

where  $E_k$  is the potential value of the cathode, and  $E_a$  is the potential value of the anode.

The power density of EFC was calculated according to equation  $P = U^2/R$  and dividing it by the geometric surface area.

The results of the power density calculations are presented in Figure 2. The highest power density was generated by the system EBFC<sub>CA</sub>. The surface power density of this system is about 2.5–4.0  $\mu\text{W}/\text{cm}^2$  (Figure 2). While the power density values generated by the other systems EBFC<sub>CC</sub>, EBFC<sub>ChV</sub>, and EBFC<sub>Hep</sub> were about 10 times lower. As expected, the power density generated by the system without any redox mediator was the lowest. Some differences were observed between the values of the carbon composite resistor load used to obtain the maximum power density. The maximum power density generated by the redox system mediated by Chlorophyll a was registered at a biofuel cell potential of +125 mV. The power density has succeeded the comparably high value in the system employing heparin, with a potential of +35 mV. The potentials generated by other biofuel cells EBFC<sub>CC</sub> and EBFC<sub>ChV</sub>, based on cytochromes and the supernatant of ultrasonically disrupted *Chlorella vulgaris* cells, were rather similar, but the potential of EBFC<sub>CC</sub> was +80 mV and of EBFC<sub>ChV</sub> was +143 mV.

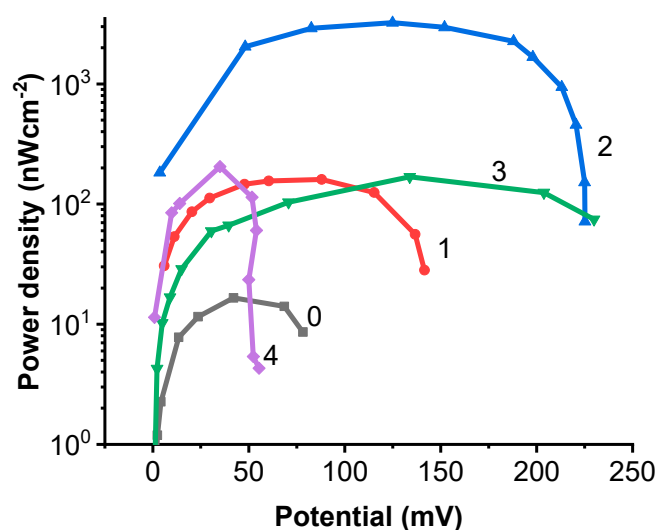


**Figure 2.** The dependencies of the maximum power density on the potential when the system is: 0—control of the study, 1—EBFC<sub>CC</sub>; 2—EBFC<sub>CA</sub>; 3—EBFC<sub>ChV</sub>; and 4—EBFC<sub>Hep</sub>.

In a similar system with a substrate of redox-mediated Chlorophyll a, a power density of 2.397  $\mu\text{W}/\text{cm}^2$  was reached using a mix of water treatment sludge and fruit juice effluent

at 3:1 [54]. In another study, the peak power densities were compared in different seasons of the year and the power density value of  $5.7 \mu\text{W}/\text{cm}^2$  was achieved in spring, and only  $0.110 \mu\text{W}/\text{cm}^2$  MFCs in summer, using biomass with the Chlorophyll a in the microbial fuel cell [55]. The biofuel cell system generated a power density of  $1.51 \mu\text{W}/\text{cm}^2$  at a glucose concentration of 20 g/l in the synthetic wastewater [56]. Biofuel cell technology is used for wastewater bio-depuration using *Chlorella vulgaris* and bio-electrogenic activity has increased from  $2.317 \mu\text{W}/\text{cm}^2$  to  $3.2767 \mu\text{W}/\text{cm}^2$  [57].

To conclude the power density evaluation, it can be noted that Chlorophyll a substrate in EBFC<sub>CA</sub> is the best choice of the assessed redox mediators used to construct the EBFC.

Five different systems were assessed by adding a particular amount of glucose to investigate the impact of glucose concentration on the power density and electromotive force of the electrochemical system, which was evaluated. Increasing glucose concentration from 0 mM and 10 mM to 100 mM (Figure 3) has decreased biofuel cell potential, and in the case of a biofuel cell based on Chlorophyll a, by increasing the glucose concentration to 100 mM, the system hardly generates power—the surface power density is very close to  $0 \mu\text{W}/\text{cm}^2$ . This effect is related to the increase in viscosity of the solution at higher glucose concentrations. Higher solution viscosity determines a significantly lower diffusion rate of glucose and redox mediators towards the active site of GOx and electrode, respectively. A similar effect at higher glucose concentrations was observed for GOx-based electrodes at higher concentrations of glucose [58]. When cytochrome c was used as the redox mediator in the EBFC<sub>CC</sub> system (Figure 3), the power generated increased with increasing glucose concentration. Although the maximum power density is lower than in EBFC<sub>CA</sub> or EBFC<sub>Ch</sub> systems and reaches about  $0.160 \mu\text{W}/\text{cm}^2$ , the signal of this system increases when the amount of glucose in the electrolyte solution has increased, and such a system was much more stable.

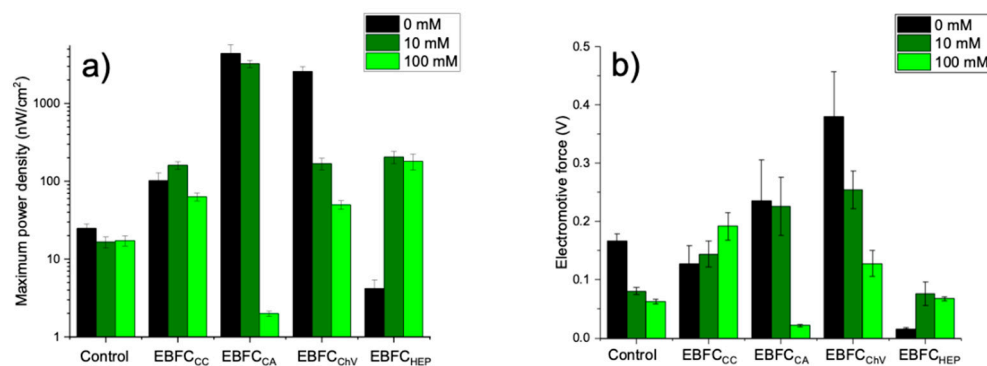


**Figure 3.** Dependences at different glucose concentrations of (a) the electric power; (b) the electromotive force of 0 control of the study; EBFC<sub>CC</sub>; EBFC<sub>CA</sub>; EBFC<sub>ChV</sub>; EBFC<sub>HeP</sub>.

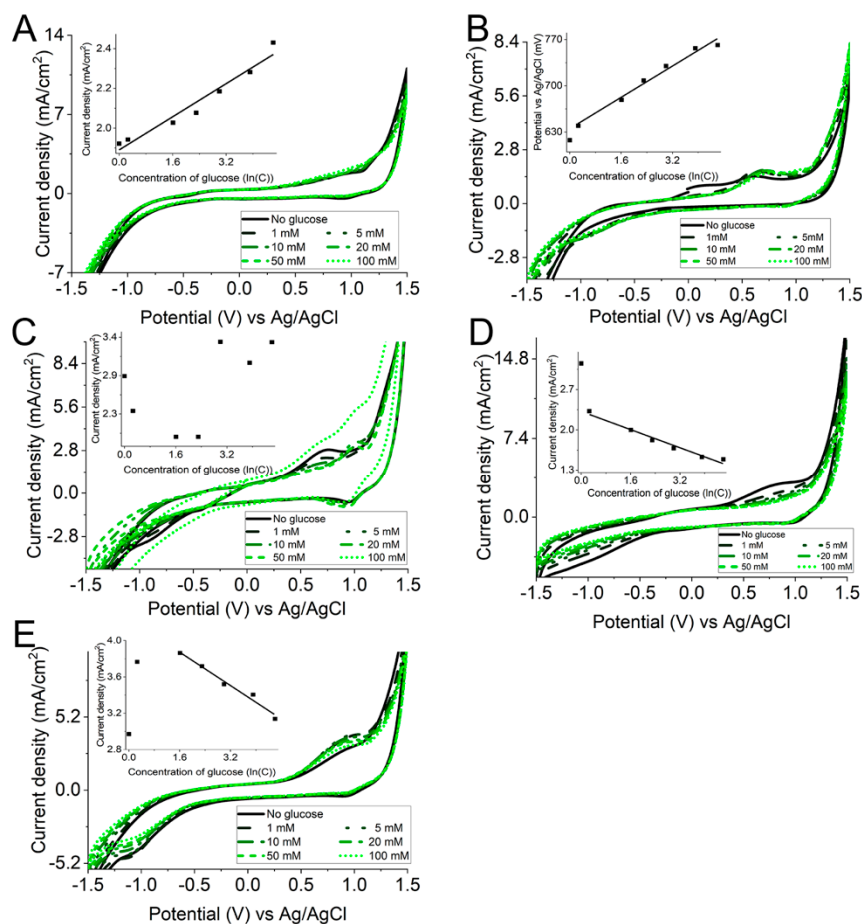
Control of the study was performed only with a polished graphite electrode—the maximum surface power density was  $0.02471 \mu\text{W}/\text{cm}^2$  in the absence of glucose in the system. Increasing glucose concentration reduces the power density of a biofuel cell. It can be argued that these redox mediators increase the efficiency of biofuel cells because they generate much higher maximum surface power.

Figure 3 compares the power density (Figure 3a) and electromotive force (Figure 3b) of all biofuel cells at a glucose concentration of 10 mM in the solution. The voltage decrease usually is registered when the load of the external circuit increases [59].

The power density of such biofuel cells is usually reported by taking into account the active surface area of the electrode, rather than volume, as is often the case for many other energy sources because more advanced calculations are not possible due to problems related to active surface calculation in the entire volume of the electrode.

### 3.2. Cyclic Voltammetry-Based Evaluation of Biofuel Cells

During the evaluation of the cyclic voltammetry results, the focus was on the value of the potential at which oxidation peak is observed in the cyclic voltammogram (CV). During this experiment the potential was changed in a rather broad range of the potential values, i.e., the potential was changed from  $-1.5$  V to  $+1.5$  V at the scan rate of  $50$  mV/s (Figure 4). The potential cycling in such a broad range of electrode potentials required the very careful removal of dissolved oxygen by degassing the electrochemical system with a nitrogen stream. It was observed that in the system without any redox mediator (Figure 4A), no clearly distinguished oxidation peak was observed. However, in this system, a slightly expressed current density increase at the potential value of  $+1.1$  V followed. The current density changes correspond to the linear correlation with  $R^2 = 0.95$  and  $y = 0.11x + 1.85$ . The current density was rather different in the evaluated EBFC systems. In the EBFC<sub>CC</sub> (Figure 4B), a shift was observed in the oxidation peak potential value. The observed potential value was shifted to higher potential values with increased glucose concentration. The potential values were shifted from  $+0.63$  V to  $+0.77$  V. Meanwhile, no current density dependence on glucose concentration was observed in this system. Such a shift of the potential value was not observed in any other evaluated system. During potential cycling at the increased glucose concentrations, a drop in the current density was observed in the EBFC<sub>CA</sub> (Figure 4C) and EBFC<sub>Hep</sub> (Figure 4E). No current or potential dependencies were observed in EBFC<sub>ChV</sub>.



**Figure 4.** Cyclic voltammograms when the working electrode is (A) control of the study; (B) EBFC<sub>CC</sub>; (C) EBFC<sub>CA</sub>; (D) EBFC<sub>ChV</sub>; and (E) EBFC<sub>Hep</sub>.

In terms of the occurrence of ineligible reactions, parasitic  $O_2$  reactions were revealed in previous research [31]. It is known that when redox mediators with highly negative

or positive redox potentials are applied, then various interfering reactions may occur depending on the experimental settings.  $O_2$  reduction at redox polymers, which is observed at low potential bioanodes, or the oxidation of some other electroactive species, which are observed at high potentials applied at biocathodes, are objectionable effects.

The values of the potential at which occurs oxidation in all evaluated systems EBFC<sub>CC</sub>, EBFC<sub>CA</sub>, EBFC<sub>ChV</sub>, and EBFC<sub>Hep</sub> are summarized in Table 1. According to the data displayed in Table 1, the value of the potential at which occurs oxidation was decreased in all systems.

**Table 1.** The summary of values of the potential at which oxidation occurs on EBFC<sub>CC</sub>, EBFC<sub>CA</sub>, EBFC<sub>ChV</sub>, and EBFC<sub>Hep</sub> electrodes.

Name of the System	The Value of the Potential at Which Oxidation Occurs, V
The control of the system	+1.1 V
EBFC <sub>CC</sub>	+0.6 V
EBFC <sub>CA</sub>	+0.8 V
EBFC <sub>ChV</sub>	+0.9 V
EBFC <sub>Hep</sub>	+0.9 V

### 3.3. Chronoamperometry-Based Evaluation of Biofuel Cells

The characteristics of the electrochemical system as a second-generation biosensor were investigated by chronoamperometry. A similarly chronoamperometric investigation of the biofuel cells was performed previously [6]. A significant difference from the cited study is that in the experiments of this work, the value of the potential was selected according to the results of the CV. EBFC<sub>CC</sub>, EBFC<sub>CA</sub>, EBFC<sub>ChV</sub>, and EBFC<sub>Hep</sub> responded to changes in glucose at a steady state. This effect is well seen from the graphs (Figure 5) that when using an EBFC<sub>ChV</sub>, a constant drop in current is observed, and the equilibrium of the system is difficult to stabilize. Due to the highly variable noise floor between samples, the LOWESS function utilizing a point interval of 10% was used to smooth out the chronoamperometric data. Using an EBFC<sub>Hep</sub>, a constant increase in current is observed. Such systems are not considered stable enough to develop a biosensor.

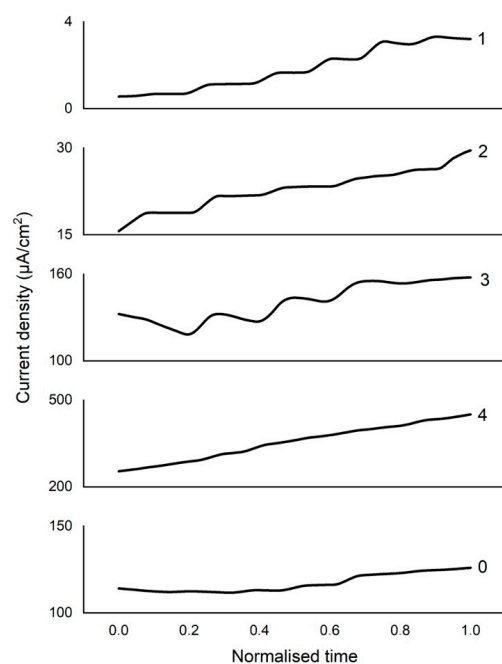


**Figure 5.** Chronoamperometry data on: 0—control of the study; 1—EBFC<sub>CC</sub>; 2—EBFC<sub>CA</sub>; 3—EBFC<sub>ChV</sub>; and 4—EBFC<sub>Hep</sub> electrodes. The LOWESS function utilizing a point interval of 10% was used.

The electrodes EBFC<sub>CA</sub> and EBFC<sub>CC</sub> were suitable for the development of EBFC. It was determined that by increasing the glucose content in the system, the current density increases, and the equilibrium is reached quickly. Due to the highly variable base levels, it is difficult to assess and compare the systems directly from the data of the chronoamperometry. Measurement results, which are presented in Figure 6, are based on the data presented in Figure 5 because by measuring the change in current density we can more easily compare the efficiency of the tested systems. All the tested systems react to the addition of glucose, gradually increased glucose concentration increases the observed change in current density by nearly a whole order of magnitude, with the highest overall increase observed in the EBFC<sub>CC</sub>, when saturated with glucose it displayed a 15-times increase in change of current density compared to the control system. The EBFC<sub>ChV</sub> also displays a large relative change in current, by over a whole order of magnitude, but appears to saturate quickly, offering a decreased response range saturating at 20 mM/L of glucose, whereas all the other tested systems displayed a change in current density throughout the tested 0–100 mM/L glucose range.

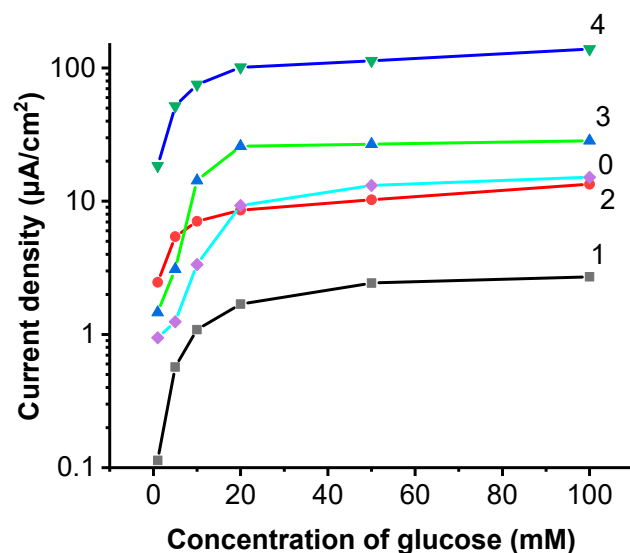


**Figure 6.** Current density dependency on glucose concentration.  $\Delta J, \log_{10}(J_i - J_0)$  from the concentration of glucose, where  $J_i$ —current density is measured after the addition of glucose, and  $J_0$ —current density is measured at the start of the experiment: 0—control of the study; 1—EBFC<sub>CC</sub>; 2—EBFC<sub>CA</sub>; 3—EBFC<sub>ChV</sub>; and 4—EBFC<sub>Hep</sub>.

All samples follow expected Michael-Menten kinetics curves. Displayed as such, EBFC<sub>Hep</sub> and ‘Control’ samples represent an inaccurate view due to the nature of their response as seen in the chronoamperometry data. Both EBFC<sub>Hep</sub> and ‘Control’ samples do not reach equilibrium and continuously increase.

The relative change in current density was calculated according to Equation (3):

$$\log_{10} \frac{J_i - J_{i-1}}{J_0 * 100\%} \quad (3)$$

where  $J_i$ —current density after the addition of glucose,  $J_{i-1}$ —current density before the addition of glucose, and  $J_0$ —current density measured at the start of the experiment.

The application of cytochromes in the EBFC<sub>CC</sub> produced the greatest relative current response to the further increase in glucose concentration. It can also be observed from Figure 7 that the system retains a high amount of sensitivity throughout the assessed concentration range, displaying the increase in registered current up to 50 mM of glucose, with further increases gradually lowering the current response rate. Increasing glucose concentration from 20 mM to 50 mM we observed a 167% increase in registered current,

by further increasing the concentration by 50 mM we observed an increase of 80%, and the response rate follows a bell-shaped curve over the entire tested concentration range. The high relative sensitivity suggests a possibility for further iterative improvement, as the system is currently held back only due to small absolute signal current values.

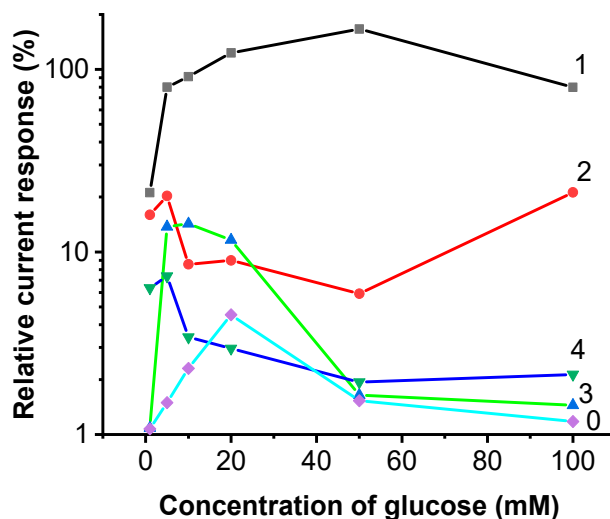


**Figure 7.** The dependence of relative change in current density from glucose concentration: 0—control; 1—EBFC<sub>CC</sub>—the system with Cytochrome c substrate; 2—EBFC<sub>CA</sub>—the system with Chlorophyll a substrate; 3—EBFC<sub>ChV</sub>—the system with the supernatant of ultrasonically disrupted *Chlorella vulgaris* cells substrate; 4—EBFC<sub>Hep</sub>—the system with heparin.

EBFC<sub>CA</sub> also produced a relatively linear current response to the increase in glucose throughout the range.

EBFC<sub>ChV</sub> displayed a strong response in the lower boundaries of the concentration range and plateaus at concentrations above 20 mM. EBFC<sub>Hep</sub> and control samples had a relatively low response to noise ratio and both samples reacted strongly in a very limited concentration range in the lower boundaries of the tested range.

#### 4. Conclusions and Future Perspectives

In this study, an enzyme-based biofuel cell system was developed and explored with different redox materials used to evaluate their applicability as redox mediators. Mediators of different natures have been selected to gain a better charge transfer in a biofuel cell and its effects on the environment and the cell as a whole system. Cytochrome c, Chlorophyll a, and the supernatant of ultrasonically disrupted *Chlorella vulgaris* cells were examined. Electron transfer between enzyme and electrode was facilitated by mediators attached to the electrode. EBFC<sub>ChV</sub> and EBFC<sub>CC</sub> were suitable for the development of EBFC. It was determined that by increasing the glucose content in the system, the current density increased, and the equilibrium was reached faster as the reaction proceeded more quickly. The power density measurements were made to evaluate generated power. The highest power was generated by the EBFC<sub>CA</sub> and EBFC<sub>ChV</sub> systems: the surface power density was about 2.5–4.0  $\mu\text{W}/\text{cm}^2$ . However, with increasing glucose concentration, these EBFC-based systems were inhibited by glucose, and in the case of EBFC<sub>CA</sub>, by increasing the glucose concentration to 100 mM, the system generated a current with a surface power density of 0  $\mu\text{W}/\text{cm}^2$ . Hence, in this research we have improved the performance of biofuel cells by a selection of better redox mediators and heparin used for electrode modifications, to improve the electron transfer in the system, and the most efficient redox mediators for future perspectives are Chlorophyll a and Cytochrome c. Published research studies [60,61] show that heparin strengthens proteins and complexes by facilitating their transport and

indirect electron transfer. Low molecular weight heparin is used as a material to coat enzymatic biofuel cells to enhance functionality [62].

In future experiments, some questions, such as the electrode material effect on the performance of EBFC, could be answered. Finally, different constructions of the electrochemical cell could be evaluated including the employment of semipermeable membranes for the separation of bioanode and biocathode.

**Author Contributions:** Conceptualization, S.Z., U.S.B., V.R. and A.R.; Methodology, S.Z.; Validation, S.Z., U.S.B. and V.L.; Formal analysis, S.Z., A.R., U.S.B. and V.R.; Investigation, S.Z. and V.L.; Resources, U.S.B. and A.R.; Data Curation, S.Z.; Writing—Original Draft, U.S.B., S.Z. and V.R.; Writing—Review and Editing, S.Z., U.S.B., V.R., M.V., I.M., A.L., V.L., M.D., S.R. and A.R.; Visualization, U.S.B., S.Z. and V.R.; Supervision, S.Z., U.S.B. and A.R.; Project administration, U.S.B.; Funding acquisition, U.S.B. and A.R. All authors have read and agreed to the published version of the manuscript.

**Funding:** This project has received funding from the European Social Fund (Project No.: 09.3.3-LMT-K-712-19-0153) under a grant agreement with the Research Council of Lithuania (LMTLT).

**Data Availability Statement:** Not applicable.

**Acknowledgments:** This project has received funding from the European Social Fund (Project No.: 09.3.3-LMT-K-712-19-0153) under a grant agreement with the Research Council of Lithuania (LMTLT). This research was supported by an inter-institutional RTO framework. The authors are grateful to Deimante Stankunaite for her help in conducting the research experiment of this study.

**Conflicts of Interest:** The authors declare no conflict of interest.

## References

1. Ramanavicius, S.; Ramanavicius, A. Conducting Polymers in the Design of Biosensors and Biofuel Cells. *Polymers* **2021**, *13*, 49. [CrossRef]
2. Mehlig, D.; ApSimon, H.; Staffell, I. The impact of the UK's COVID-19 lockdowns on energy demand and emissions. *Environ. Res. Lett.* **2021**, *16*, 054037. [CrossRef]
3. Kikstra, J.S.; Vinca, A.; Lovat, F.; Boza-Kiss, B.; van Ruijven, B.; Wilson, C.; Rogelj, J.; Zakeri, B.; Fricko, O.; Riahi, K. Climate mitigation scenarios with persistent COVID-19-related energy demand changes. *Nat. Energy* **2021**, *6*, 1114–1123. [CrossRef]
4. Rouleau, J.; Gosselin, L. Impacts of the COVID-19 lockdown on energy consumption in a Canadian social housing building. *Appl. Energy* **2021**, *287*, 116565. [CrossRef]
5. Ramanavicius, S.; Ramanavicius, A. Charge Transfer and Biocompatibility Aspects in Conducting Polymer-Based Enzymatic Biosensors and Biofuel Cells. *Nanomaterials* **2021**, *11*, 371. [CrossRef]
6. Kisieliute, A.; Popov, A.; Apetrei, R.-M.; Cârâc, G.; Morkvenaite-Vilkonciene, I.; Ramanaviciene, A.; Ramanavicius, A. Towards microbial biofuel cells: Improvement of charge transfer by self-modification of microorganisms with conducting polymer-polyppyrrole. *Chem. Eng. J.* **2019**, *356*, 1014–1021. [CrossRef]
7. Ramanavicius, A.; Kausaite-Minkstiniene, A.; Morkvenaite-Vilkonciene, I.; Genys, P.; Mikhailova, R.; Semashko, T.; Voronovic, J.; Ramanaviciene, A. Biofuel cell based on glucose oxidase from *Penicillium funiculosum* 46.1 and horseradish peroxidase. *Chem. Eng. J.* **2015**, *264*, 165–173. [CrossRef]
8. Pant, D.; Van Bogaert, G.; Diels, L.; Vanbroekhoven, K. A review of the substrates used in microbial fuel cells (MFCs) for sustainable energy production. *Bioresour. Technol.* **2010**, *101*, 1533–1543. [CrossRef]
9. Yuan, W.; Zhang, J.; Shen, P.K.; Li, C.M.; Jiang, S.P. Self-assembled CeO<sub>2</sub> on carbon nanotubes supported Au nanoclusters as superior electrocatalysts for glycerol oxidation reaction of fuel cells. *Electrochimica Acta* **2016**, *190*, 817–828. [CrossRef]
10. Karajic, A.; Merzeau, P.; Suraniti, E.; Gounel, S.; Jaillet, C.; Kuhn, A.; Mano, N. Enzymatic Glucose-Oxygen Biofuel Cells for Highly Efficient Interfacial Corrosion Protection. *ACS Appl. Energy Mater.* **2020**, *3*, 4441–4448. [CrossRef]
11. Karim, N.A.; Yang, H. Mini-Review: Recent Technologies of Electrode and System in the Enzymatic Biofuel Cell (EBFC). *Appl. Sci.* **2021**, *11*, 5197. [CrossRef]
12. Rewatkar, P.; Kothuru, A.; Goel, S. PDMS-Based Microfluidic Glucose Biofuel Cell Integrated With Optimized Laser-Induced Flexible Graphene Bioelectrodes. *IEEE Trans. Electron Devices* **2020**, *67*, 1832–1838. [CrossRef]
13. Qiang, L.; Yuan, L.-J.; Ding, Q. Influence of buffer solutions on the performance of microbial fuel cell electricity generation. *Huan Jing Ke Xue* **2011**, *32*, 1524–1528.
14. Mukherjee, S.; Ganguly, A.; Ghosh, A. A comparative study on the energy generation through wastewater purification in microbial fuel cell. *Mater. Today Proc.* **2022**, *57*, 1682–1686. [CrossRef]
15. Kwon, C.H.; Ko, Y.; Shin, D.; Kwon, M.; Park, J.; Bae, W.K.; Lee, S.W.; Cho, J. High-power hybrid biofuel cells using layer-by-layer assembled glucose oxidase-coated metallic cotton fibers. *Nat. Commun.* **2018**, *9*, 4479. [CrossRef]

16. Anson, C.W.; Stahl, S.S. Mediated Fuel Cells: Soluble Redox Mediators and Their Applications to Electrochemical Reduction of O<sub>2</sub> and Oxidation of H<sub>2</sub>, Alcohols, Biomass, and Complex Fuels. *Chem. Rev.* **2020**, *120*, 3749–3786. [[CrossRef](#)]
17. Zhong, X.; Yuan, W.; Kang, Y.; Xie, J.; Hu, F.; Li, C.M. Biomass-Derived Hierarchical Nanoporous Carbon with Rich Functional Groups for Direct-Electron-Transfer-Based Glucose Sensing. *ChemElectroChem* **2015**, *3*, 144–151. [[CrossRef](#)]
18. Haque, S.U.; Duteanu, N.; Ciocan, S.; Nasar, A. Inamuddin A review: Evolution of enzymatic biofuel cells. *J. Environ. Manag.* **2021**, *298*, 113483. [[CrossRef](#)]
19. German, N.; Ramanavicius, A.; Ramanaviciene, A. Amperometric Glucose Biosensor Based on Electrochemically Deposited Gold Nanoparticles Covered by Polypyrrole. *Electroanalysis* **2017**, *29*, 1267–1277. [[CrossRef](#)]
20. German, N.; Ramanaviciene, A.; Ramanavicius, A. Dispersed Conducting Polymer Nanocomposites with Glucose Oxidase and Gold Nanoparticles for the Design of Enzymatic Glucose Biosensors. *Polymers* **2021**, *13*, 2173. [[CrossRef](#)]
21. Yuan, W.; Lu, S.; Xiang, Y.; Jiang, S.P. Pt-based nanoparticles on non-covalent functionalized carbon nanotubes as effective electrocatalysts for proton exchange membrane fuel cells. *RSC Adv.* **2014**, *4*, 46265–46284. [[CrossRef](#)]
22. Ramanavicius, A.; Ramanaviciene, A. Hemoproteins in Design of Biofuel Cells. *Fuel Cells* **2009**, *9*, 25–36. [[CrossRef](#)]
23. Giroud, F.; Gondran, C.; Gorgy, K.; Vivier, V.; Cosnier, S. An enzymatic biofuel cell based on electrically wired polyphenol oxidase and glucose oxidase operating under physiological conditions. *Electrochimica Acta* **2012**, *85*, 278–282. [[CrossRef](#)]
24. Cinquin, P.; Gondran, C.; Giroud, F.; Mazabrard, S.; Pellissier, A.; Boucher, F.; Alcaraz, J.-P.; Gorgy, K.; Lenouvel, F.; Mathé, S.; et al. A Glucose BioFuel Cell Implanted in Rats. *PLoS ONE* **2010**, *5*, e10476. [[CrossRef](#)]
25. Trifonov, A.; Herkendell, K.; Tel-Vered, R.; Yehezkeili, O.; Woerner, M.; Willner, I. Enzyme-Capped Relay-Functionalized Mesoporous Carbon Nanoparticles: Effective Bioelectrocatalytic Matrices for Sensing and Biofuel Cell Applications. *ACS Nano* **2013**, *7*, 11358–11368. [[CrossRef](#)]
26. Rozene, J.; Morkvenaite-Vilkonciene, I.; Bruzaite, I.; Zinovicius, A.; Ramanavicius, A. Baker's Yeast-Based Microbial Fuel Cell Mediated by 2-Methyl-1,4-Naphthoquinone. *Membranes* **2021**, *11*, 182. [[CrossRef](#)]
27. Zinovicius, A.; Rozene, J.; Merkeli, T.; Bruzaite, I.; Ramanavicius, A.; Morkvenaite-Vilkonciene, I. Evaluation of a Yeast-Polypyrrole Biocomposite Used in Microbial Fuel Cells. *Sensors* **2022**, *22*, 327. [[CrossRef](#)]
28. Mardiana, U.; Innocent, C.; Jarrar, H.; Cretin, M.; Gandasasmita, S. Electropolymerized neutral red as redox mediator for yeast fuel cell. *Int. J. Electrochem. Sci.* **2015**, *10*, 8886–8898.
29. Ben Tahar, A.; Szymczyk, A.; Tingry, S.; Vadgama, P.; Zelsmanne, M.; Tsujumura, S.; Cinquin, P.; Martin, D.; Zebda, A. One-year stability of glucose dehydrogenase confined in a 3D carbon nanotube electrode with coated poly-methylene green: Application as bioanode for a glucose biofuel cell. *J. Electroanal. Chem.* **2019**, *847*, 113069. [[CrossRef](#)]
30. Zumpano, R.; Lambertini, L.; Tortolini, C.; Bollella, P.; Favero, G.; Antiochia, R.; Mazzei, F. A glucose/oxygen enzymatic fuel cell exceeding 1.5 V based on glucose dehydrogenase immobilized onto polyMethylene blue-carbon nanotubes modified double-sided screen printed electrodes: Proof-of-concept in human serum and saliva. *J. Power Sources* **2020**, *476*, 228615. [[CrossRef](#)]
31. Conzuelo, F.; Markovic, N.; Ruff, A.; Schuhmann, W. The Open Circuit Voltage in Biofuel Cells: Nernstian Shift in Pseudocapacitive Electrodes. *Angew. Chem. Int. Ed.* **2018**, *57*, 13681–13685. [[CrossRef](#)] [[PubMed](#)]
32. Everse, J. Heme Proteins. In *Encyclopedia of Biological Chemistry*, 2nd ed.; Lennarz, W.J., Lane, M.D., Eds.; Academic Press: Waltham, MA, USA, 2013; pp. 532–538.
33. Kumari, A. Chapter 3-Electron Transport Chain. In *Sweet Biochemistry*; Kumari, A., Ed.; Academic Press: Cambridge, MA, USA, 2018; pp. 13–16.
34. Hemker, H.C. A century of heparin: Past, present and future. *J. Thromb. Haemost.* **2016**, *14*, 2329–2338. [[CrossRef](#)] [[PubMed](#)]
35. Lima, M.; Rudd, T.; Yates, E. New Applications of Heparin and Other Glycosaminoglycans. *Molecules* **2017**, *22*, 749. [[CrossRef](#)] [[PubMed](#)]
36. Atallah, J.; Khachfe, H.H.; Berro, J.; Assi, H.I. The use of heparin and heparin-like molecules in cancer treatment: A review. *Cancer Treat. Res. Commun.* **2020**, *24*, 100192. [[CrossRef](#)] [[PubMed](#)]
37. Partridge, L.; Urwin, L.; Nicklin, M.; James, D.; Green, L.; Monk, P. ACE2-Independent Interaction of SARS-CoV-2 Spike Protein with Human Epithelial Cells Is Inhibited by Unfractionated Heparin. *Cells* **2021**, *10*, 1419. [[CrossRef](#)]
38. Qiu, M.; Glass, Z.; Chen, J.; Haas, M.; Jin, X.; Zhao, X.; Rui, X.; Ye, Z.; Li, Y.; Zhang, F.; et al. Lipid nanoparticle-mediated codelivery of Cas9 mRNA and single-guide RNA achieves liver-specific in vivo genome editing of *Angptl*. *Proc. Natl. Acad. Sci. USA* **2021**, *118*, e2020401118. [[CrossRef](#)]
39. Singh, A.K.; Rana, H.K.; Pandey, A.K. Chapter 19-Analysis of chlorophylls. In *Recent Advances in Natural Products Analysis*; Sanches Silva, A., Nabavi, S.F., Saeedi, M., Nabavi, S.M., Eds.; Elsevier: Amsterdam, The Netherlands, 2020; pp. 635–650.
40. Ropp, R.C. *Encyclopedia of the Alkaline Earth Compounds*; Elsevier: Amsterdam, The Netherlands, 2013.
41. Pareek, S.; Sagar, N.A.; Sharma, S.; Kumar, V.; Agarwal, T.; González-Aguilar, G.A.; Yahia, E.M. Chlorophylls: Chemistry and Biological Functions. In *Fruit and Vegetable Phytochemicals: Chemistry and Human Health*; Wiley: Hoboken, NJ, USA, 2017; pp. 269–284. [[CrossRef](#)]
42. Lu, C.; Xie, Z.; Guo, J.; Song, Y.; Xing, Y.; Han, Y.; Li, H.; Hou, Y. Chlorophyll as natural redox mediators for the denitrification process. *Int. Biodeterior. Biodegrad.* **2020**, *148*, 104895. [[CrossRef](#)]
43. Mandal, R.; Dutta, G. From photosynthesis to biosensing: Chlorophyll proves to be a versatile molecule. *Sensors Int.* **2020**, *1*, 100058. [[CrossRef](#)]

44. Ullah, K.; Ahmad, M.; Sharma, V.K.; Lu, P.; Harvey, A.; Zafar, M.; Sultana, S.; Anyanwu, C. Algal biomass as a global source of transport fuels: Overview and development perspectives. *Prog. Nat. Sci.* **2014**, *24*, 329–339. [[CrossRef](#)]
45. Jadhav, D.A.; Carmona-Martínez, A.A.; Chendake, A.D.; Pandit, S.; Pant, D. Modeling and optimization strategies towards performance enhancement of microbial fuel cells. *Bioresour. Technol.* **2020**, *320*, 124256. [[CrossRef](#)]
46. Khandelwal, A.; Vijay, A.; Dixit, A.; Chhabra, M. Microbial fuel cell powered by lipid extracted algae: A promising system for algal lipids and power generation. *Bioresour. Technol.* **2018**, *247*, 520–527. [[CrossRef](#)] [[PubMed](#)]
47. Yadav, G.; Shanmugam, S.; Sivaramakrishnan, R.; Kumar, D.; Mathimani, T.; Brindhadevi, K.; Pugazhendhi, A.; Rajendran, K. Mechanism and challenges behind algae as a wastewater treatment choice for bioenergy production and beyond. *Fuel* **2020**, *285*, 119093. [[CrossRef](#)]
48. Song, X.; Wang, W.; Cao, X.; Wang, Y.; Zou, L.; Ge, X.; Zhao, Y.; Si, Z.; Wang, Y. Chlorella vulgaris on the cathode promoted the performance of sediment microbial fuel cells for electrogenesis and pollutant removal. *Sci. Total Environ.* **2020**, *728*, 138011. [[CrossRef](#)] [[PubMed](#)]
49. Kumar, P.K.; Krishna, S.V.; Naidu, S.S.; Verma, K.; Bhagawan, D.; Himabindu, V. Biomass production from microalgae Chlorella grown in sewage, kitchen wastewater using industrial CO<sub>2</sub> emissions: Comparative study. *Carbon Resour. Convers.* **2019**, *2*, 126–133. [[CrossRef](#)]
50. Koekkoek, L.L.; Mul, J.D.; la Fleur, S.E. Glucose-Sensing in the Reward System. *Front. Neurosci.* **2017**, *11*, 716. [[CrossRef](#)]
51. Ramanavicius, A.; Kausaite, A.; Ramanaviciene, A. Biofuel cell based on direct bioelectrocatalysis. *Biosens. Bioelectron.* **2005**, *20*, 1962–1967. [[CrossRef](#)]
52. Krikstolaityte, V.; Oztekin, Y.; Kuliesius, J.; Ramanaviciene, A.; Yazicigil, Z.; Ersoz, M.; Okumus, A.; Kausaite-Minkstimiene, A.; Kilic, Z.; Solak, A.O.; et al. Biofuel Cell Based on Anode and Cathode Modified by Glucose Oxidase. *Electroanalysis* **2013**, *25*, 2677–2683. [[CrossRef](#)]
53. Žalnėravičius, R.; Paškevičius, A.; Samukaitė-Bubnienė, U.; Ramanavičius, S.; Vilkienė, M.; Mockevičienė, I.; Ramanavičius, A. Microbial Fuel Cell Based on Nitrogen-Fixing *Rhizobium anhuiense* Bacteria. *Biosensors* **2022**, *12*, 113. [[CrossRef](#)]
54. del Campo, A.G.; Perez, J.F.; Cañizares, P.; Rodrigo, M.A.; Fernandez, F.J.; Lobato, J. Study of a photosynthetic MFC for energy recovery from synthetic industrial fruit juice wastewater. *Int. J. Hydrogen Energy* **2014**, *39*, 21828–21836. [[CrossRef](#)]
55. Mohan, S.V.; Srikanth, S.; Chiranjeevi, P.; Arora, S.; Chandra, R. Algal biocathode for in situ terminal electron acceptor (TEA) production: Synergetic association of bacteria–microalgae metabolism for the functioning of biofuel cell. *Bioresour. Technol.* **2014**, *166*, 566–574. [[CrossRef](#)]
56. Yakar, A.; Türe, C.; Türker, O.C.; Vymazal, J.; Saz, Ç. Impacts of various filtration media on wastewater treatment and bioelectric production in up-flow constructed wetland combined with microbial fuel cell (UCW-MFC). *Ecol. Eng.* **2018**, *117*, 120–132. [[CrossRef](#)]
57. Huarachi-Olivera, R.; Dueñas-Gonza, A.; Yapo-Pari, U.; Vega, P.; Romero-Ugarte, M.; Tapia, J.; Molina, L.; Lazarte-Rivera, A.; Pacheco-Salazar, D.; Esparza, M. Bioelectrogenesis with microbial fuel cells (MFCs) using the microalga Chlorella vulgaris and bacterial communities. *Electron. J. Biotechnol.* **2018**, *31*, 34–43. [[CrossRef](#)]
58. Zor, E.; Oztekin, Y.; Ramanaviciene, A.; Anusevicius, Z.; Voronovic, J.; Bingol, H.; Barauskas-Memenas, D.; Labanauskas, L.; Ramanavicius, A. Evaluation of 1,10-phenanthroline-5,6-dione as redox mediator for glucose oxidase. *J. Anal. Chem.* **2015**, *71*, 77–81. [[CrossRef](#)]
59. Malekmohammadi, S.; Mirbagheri, S.A. A review of the operating parameters on the microbial fuel cell for wastewater treatment and electricity generation. *Water Sci. Technol.* **2021**, *84*, 1309–1323. [[CrossRef](#)] [[PubMed](#)]
60. Fatma, N.; Singh, D.P.; Shinohara, T.; Chylack, L.T., Jr. Heparin's Roles in Stabilizing, Potentiating, and Transporting LEDGF into the Nucleus. *Investig. Ophthalmol. Vis. Sci.* **2000**, *41*, 2648–2657.
61. Quarto, N.; Amalric, F. Heparan sulfate proteoglycans as transducers of FGF-2 signalling. *J. Cell Sci.* **1994**, *107*, 3201–3212. [[CrossRef](#)]
62. Xu, X.; Dai, Y. Heparin: An intervenor in cell communication. *J. Cell. Mol. Med.* **2009**, *14*, 175–180. [[CrossRef](#)]